International Journal of Advanced Research in Physical Science (IJARPS)
Volume 10, Issue 5, 2023, PP 1-16
ISSN No. (Online) 2349-7882
www.arcjournals.org

To Question about Nature of Laser-Induced Cavitation

Petro P. Trokhimchuck*

Anatoliy Svidzinskii Department of Theoretical and Computer Physics, Lesya Ukrayinka Eastern European National University, 13 Voly Avenue, 43025, Lutsk, Ukraine.

Corresponding Author:** ***Petro P. Trokhimchuck, *Anatoliy Svidzinskii Department of Theoretical and Computer Physics, Lesya Ukrayinka Eastern European National University, 13 Voly Avenue, 43025, Lutsk, Ukraine.*

Abstract: *Main peculiarities of laser-induced cavitation are discussed. Shiort review of corresponding experimental data is represented. Corresponding models and theories, which are used for the explanation this phenomenon, are represented. The main focus is on the Rayleigh model and its modifications. The issue of the nature and conditions of obtaining laser-optical and laser-acoustic cavitation was investigated. The given models make it possible to explain the corresponding experimental data.*

Keywords: *cavitation, optical breakdown, Rayleygh, Relaxed Optics, acoustic, cascade processes, laser irradiation, filaments, liquids, solid.*

1. INTRODUCTION

Cavitation**,** formation of vapour bubbles within a liquid at low-pressure regions that occur in places where the liquid has been accelerated to high velocities, as in the operation of centrifugal pumps, water turbines, and marine propellers. Cavitation is undesirable because it produces extensive erosion of the rotating blades, additional noise from the resultant knocking and vibrations, and a significant reduction of efficiency because it distorts the flow pattern [1-5]. The cavities form when the pressure of the liquid has been reduced to its vapour pressure; they expand as the pressure is further reduced along with the flow and suddenly collapse when they reach regions of higher pressure. The sudden growth and collapse of these vapour cavities cause the extreme pressures that pit the metal surfaces exposed to the cavitating liquid [1-5].

Laser-induced cavitation occurs, as a rule, during the optical breakdown of matter and is observed in liquids and solids. Therefore, corresponding experimental experimental data are represented for liquid and solid [6-25].

Short analysis of Rayleygh theory of cavitation and its extensions (Rayleigh–Plesset, Gilmore and Keller–Miksis models) are made [5, 20]. These models are not include the prehistory of these processes. Therefore, we include cascade theory of laser-induced optical breakdown as theory which include the prehistory and cavitation.

Main peculiarity of laser-induced optical breakdown it is the transformation initial laser radiation from long-wave into short-wave, which is effectively absorbed in the near-surface layers, which leads to optical breakdown and the generation of cavitation bubbles [7-10, 15].

Unlike the plasma and thermal models of laser-induced optical breakdown, where the main problem is to find seed inhomogeneities in the material that intensively absorb light that is weakly absorbed by the irradiated material, the cascade model takes into account the cascade of transformations of optical radiation from impurity (long-wave) to intrinsic (short-wave) radiation. Therefore, for the cascade model, the inhomogeneity of the irradiated material is unnecessary, as this inhomogeneity is formed by the cascade of transformations of the output radiation.

The problem of observation the shork directed (ordered quantum) and disordered electromagnetic processes [6-10, 15] is one of main problems in Nonlinear and Relaxed Optics. First processes have local short range action coherent nature. They are caused by direct short-term chain processes of scattering (absorption) of light directly in the coherent zone of interaction. Therefore, these processes have a clearly defined orientation character and kinetic nature. Second processes have dynamical nature and do not have such a clearly expressed orientation dependence. First processes are the classical

nonlinear optical phenomena, including Cherenkov radiation [26, 27] and shock laser-induced optical breakdown of matter [7-10, 15]. Second processes are represented noneequilibrium and irreversible plasma and simple to it processes.

This model include chain of next processes: diffraction stratification, surface generation of Cherenkov radiation on each cone of diffractive stratification, interference of short-wave part of Cherenkov radiation and optical breakdown in the maximum of this interferogram [7-10, 15]]. Questions related to the nature and difference of electromagnetic and acoustic impact processes are also discussed.

2. EXPERIMENTAL DATA

Many of the measurement techniques used to characterize filaments rely on the assumption that the physical phenomena involved in filamentation keep a clear separation between spatial and temporal effects. Filament are therefore often characterized in terms of pulse duration, beam diameter, peak intensity, and averaged quantities such as the fluence (time integrated intensity) or the power. When strong coupling between space and time occurs as in the generation of filaments, many of these concepts, however, lose their meaning.

Recently, evidence of strong space–time coupling was revealed by use of an imaging spectrometer allowing a map of the far-field angular spectra of 200-*fs* optical pulses that have undergone beam collapse and filamentation in a Kerr solid or liquid [16, 17, 20] . The far-fields exhibit an X-shape and a strong modulated on-axis emission (Fig. 1a)). This fringe pattern was observed by studying the evolution of the spectra with increasing input powers, revealing the complexity of the space time coupled phenomena from angular-spectral characterization. He et al. [20] characterized the conical emission in Kerr and non-Kerr liquids pumped with ultrashort laser pulses and observed X-shaped angular spectra. These X-shaped angular spectra were reinterpreted only recently as a manifestation of the spontaneous dynamics of ultrashort laser pulses undergoing filamentation, which tends to generate a stationary conical wave [20]. An analysis of the role of nonlinear losses in the filament dynamics was made in the framework of a monochromatic approach, where the role of chromatic dispersion was neglected [20]. In this case, a theoretical analysis confirmed the existence of weakly localized conical stationary solutions to the nonlinear Schrödinger equation in the presence of multiphoton absorption [20]).

In contrast, nonlinear X waves represent conical stationary solutions to the nonlinear Schrödinger equation in the presence of chromatic dispersion but when nonlinear losses are neglected; nonlinear X-waves are expected to be robust against nonlinear losses and the corresponding solutions to an extended nonlinear Schrödinger model fully accounting for nonlinear losses and chromatic dispersion should play the role of attractors for the dynamics of filamentation. Paolo Di Trapani of the University of Insubria in Como, Italy, and his collaborators discovered they could send short, intense laser pulses through a transparent crystal of lithium triborate without the pulses' typical spreading [20]. In the Como experiment, the pulses emerged from the laser aperture with the usual Gaussian profile. But when they encountered the dispersive medium of the crystal, nonlinear interactions spontaneously transformed them into a new shape that in longitudinal cross section looks like an X. Fig. 1 a) shows an example.

Nonspreading "X waves" had been created before, but in the lower-power linear regime using special equipment. In the nonlinear regime, by contrast, the X wave appears to embody a naturally occurring mode of the light–matter interaction (Fig. 1 b)) [20].

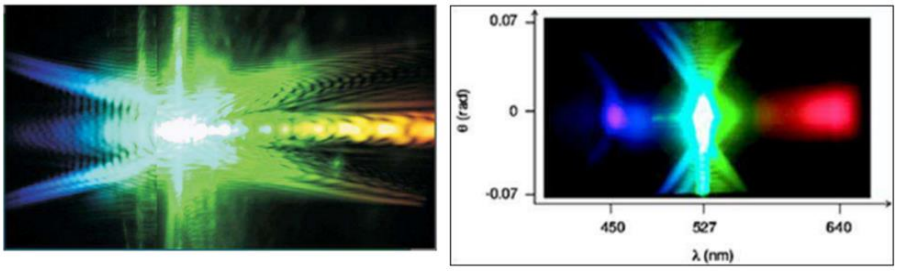

Fig1. *a) Nonlinear X waves retain their characteristic profiles when measured in Fourier space. To make this image, an X wave was sent through a lens and onto a spectrograph. The horizontal axis is angular frequency and*

the vertical axis is wave number [16, 17, 20]; ***b)*** *Double X θ.ß spectrum of a 527 nm, 3 µJ laser pulse undergoing filamentation in water. Each X-pattern exhibits a gap in frequency characterizing the velocity of each split pulse. The reduced visibility of the red tail was attributed to the increased absorption at the wavelengths [20].*

By studying the conical emission of a blue femtosecond laser filament in air, it is shown that self-improvement of the beams' spatial mode quality occurs for a self-guided laser pulse (Fig. 2) [20].

Fig. 3 show conical emission accompanying a self-guided pulse for various regimes of irradiation [28].

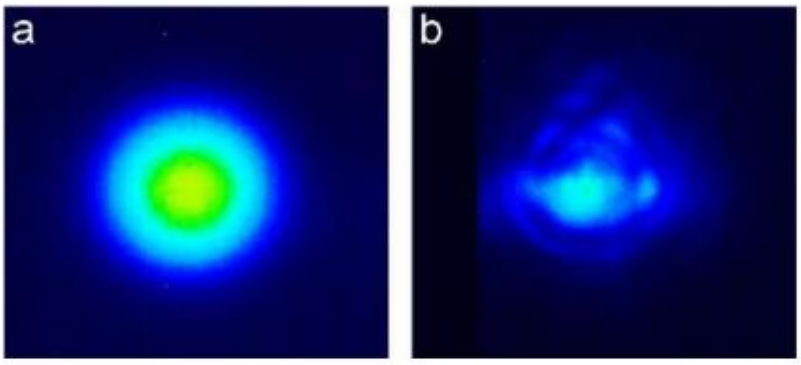

Fig2. *Conical emission and laser pattern measured after 20 m of propagation in air from a 400 nm laser pulse. (a) Surrounding conical emissiononly, with the power spectrum close to that of the incident laser pulse removed by a colour filter. The external diameter of the blue ring is about1 cm. (b) strongly attenuated total laser beam at the same distance [20].*

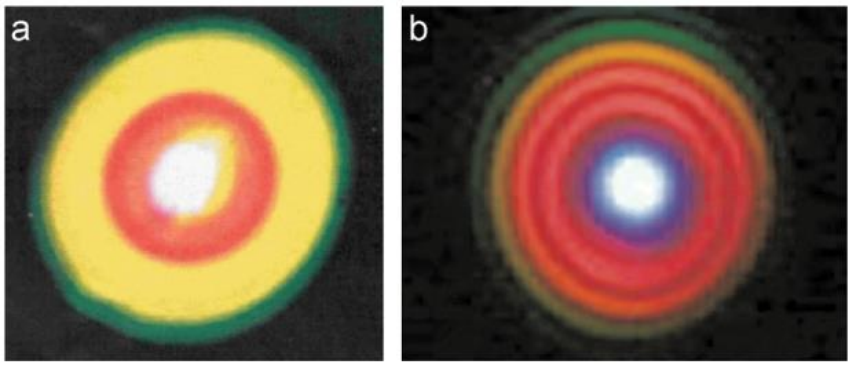

Fig3. *Conical emission accompanying a self-guided pulse. (a) A central white core (the filament) is surrounded by Newton's rings having a divergence of the order of the mrad [28]. (b) Conical emission measured at 25 m from a 5 mJ, 45 fs, 800 nm pulse [28].*

'Two damages region in a crystal with moderately high density of inclusions were received in [12] for potassium chloride KCl after irradiation by CO_2-laser pulses (wavelength 10,6 µm, duration of pulse 30 *ns*). The laser was known to be operating in the lowest-order transverse Gaussian mode. There were several longitudinal modes, however, which contributed a time structure to the pulse, periodic at the cavity round-trip time. The phase relationships between the longitudinal modes varied from shot to shot, changing the details of the time structure and causing the peak of the envelope to fluctuate by ±15% [12]. These results are presented in Fig. 4 [12].

Successive laser shot (1/sec) were focused into bulk single crystals using a 1-inch focal length "Irtran 2" lens. The breakdown was monitored by observing the visible light from the focal region and by examining the damaged region under the microscope. It was found that most of the crystals suffered some damage even at relatively low power levels. The threshold of this type of damage varied by an order magnitude from one position in the crystal to another. At any particular energy level, damage would occur on the first laser shot or not at all. Fig. 4 (a) shows that spatial inhomogeneities are in fact inclusions [12]. The damage bubbles occur randomly near, not necessarily in, the tiny focal volume. At a well-defined power threshold, an elongated pointed bubble forms, its vertex falling at the focus (Fig. 4 (b)). This power level is regarded as the bulk intrinsic breakdown threshold. Its value is reproducible in crystals from different manufacturers, with inclusions or without. When no inclusion free samples of a compound were available, the considerations mentioned above were using to determine the dielectric strength [12].

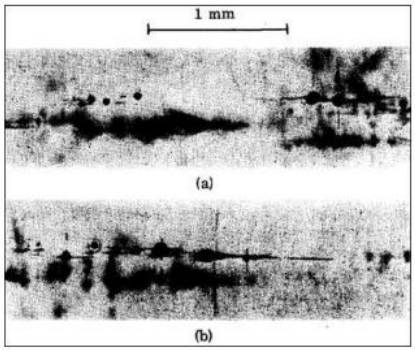

Fig4. *Two damages region in a crystal KCl with moderately high density of inclusions. The round black objects are bubbles. The radiation, incident from left to right, was yust at the intrinsic breakdown threshold. In one case (a) there was damage only at the inclusions. In (b), intrinsic breakdown occurred as evidenced by the pointed bubble. The straight lines represent cleavage [12]*

Experimental data, which are included microscopic structure of optical breakdown, are represented in Fig. 5. Sectional area of receiving structures was ~ 22 μm, the depth of ~ 50 μm. As seen from Fig. 5 (c) we have five stages disordered regions, which are located at a distance from 2 to 4 μm apart vertically [18, 19]. Branches themselves in this case have a thickness from 150 to 300 nm. In this case there are lines in the irradiated nanocavity with spherical diameter of from 10 *nm* to 20 *nm*. In this case irradiated structures have crystallographic symmetry of the initial structure. In this case diffraction processes may be generated in two stages: 1- formation of diffraction rings of focused beams [7, 8] and second- formation of diffracting gratings in the time of redistribution of second-order Cherenkov radiation [7, 8] . Second case is analogous to the creation of self-diffraction gratings in NLO, but for Fig. 5 (c) and Fig. 6 (b) our gratings are limited by much cone of Cherenkov radiation. Roughly speaking only Fig 5 (e) and Fig. 6 are represented "clean" breakdown.

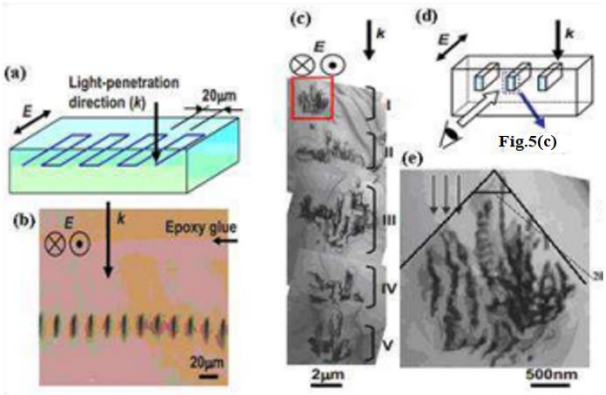

Fig5. *(a) Schematic illustration of the laser irradiated pattern. The light propagation direction (k) and electric field (E) are shown.* ***(b)*** *Optical micrograph of the mechanically thinned sample to show cross sections of laser-irradiated lines (200 nJ/pulse).* ***(c)*** *Bright-field TEM image of the cross section of a line written with pulse energy of 300 nJ/pulse.* ***(d)*** *Schematic illustration of a geometric relationship between the irradiated line and the cross-sectional micrograph.* ***(e)*** *Magnified image of a rectangular area in* ***(c)*** *[18, 19].*

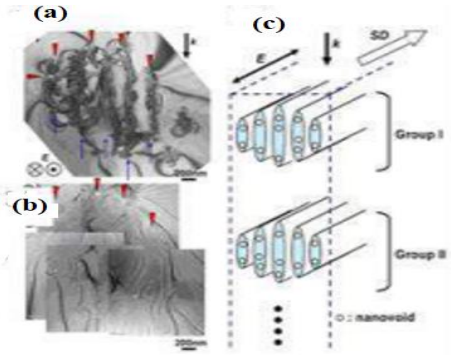

Fig6. *Laser-modified layers with a spacing of 150 nm are indicated by arrows. (a) Bright-field TEM image of a portion of the cross section of a line written with a pulse energy of 200 nJ/pulse. (b) Zero-loss image of a same*

area as in (a) with nanovoids appearing as bright areas. Correspondence with (a) is found by noting the arrowheads in both micrographs. (c) Schematic illustrations of the microstructure of a laser modified line. Light-propagation direction (k), electric field (E), and scan direction (SD) are shown. Only two groups (groups I and II) of the laser-modified microstructure are drawn [18, 19].

Photographic series of a laser produced bubble in water are shown in Fig. 7. The series starts 10μs after optical breakdown, i.e. bubble generation, and proceeds with 10μs interframe time. Maximum bubble radius is about 750 μm [20].

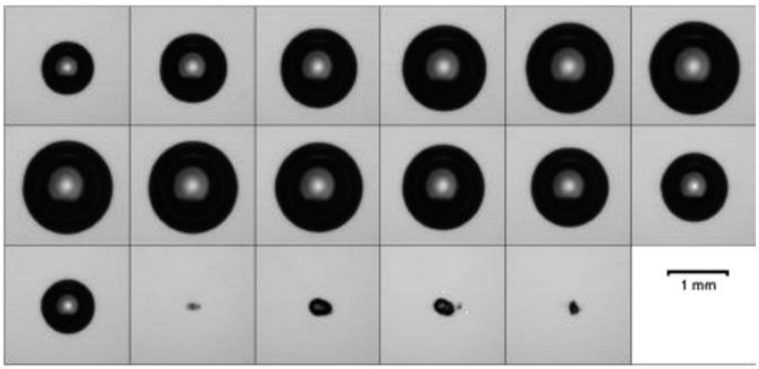

Fig7. *Photographic series of a laser produced bubble in water. The series starts 10μs after optical breakdown, i.e. bubble generation, and proceeds with 10μs interframe time. Maximum bubble radius is about 750μm [20].*

Bubble asymmetry, induced by the nonspherical shape of the laser plasma, is minimized, when the bubble is generated at the beginning of the positive pressure cycle of the sound wave. The bubble is then compressed first and stays small for some time, so that the higher surface tension pressure for smaller bubble radii can act longer in conjunction with dissipation to form a spherical bubble. Fig. 8 shows this result. A small spherical bubble as obtained without sound (Fig. 8, left frame [20]) is expanded to larger and larger radii with increasing sound pressure amplitude thereby staying highly spherical.

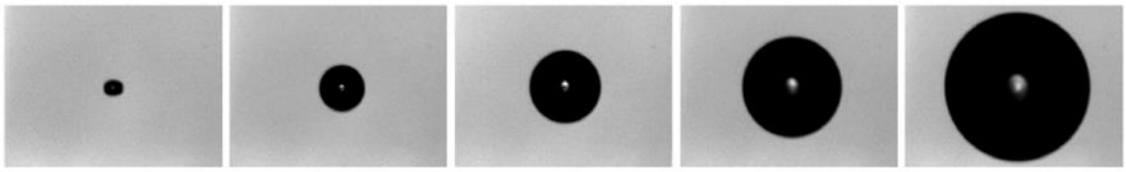

Fig8. *Laser induced bubble in a sound field of 43.68 kHz photographed at maximum expansion with increased sound pressure amplitudes (from left to right): no sound (0 bar), 1.76, 2.28, 3.12, 4.65 bar. The static pressure is p_{stat} = 1 bar. The image width is 454 μm. Bubble generation with a femtosecond laser pulse is effected at the beginning of the positive pressure cycle of the sound wave [20].*

3. MODELING AND DISCUSSIONS

The main extensions of Rayleigh's theory are Rayleigh–Plesset, Gilmore; and Keller–Miksis models.'

The creation of this theory is connected with Besant problem, which is formulated as "An infinite mass of homogeneous incompressible fluid acted upon by no forces is at rest, and a spherical portion of the fluid is suddenly annihilated; it is required to find the instantaneous alteration of pressure at any point of the mass, and the time in which the cavity will be filled up, the pressure at an infinite distance being supposed to remain constant" [5].

According to Raylegh the time of bubble collapse is determined as [5]

$$\tau = \sqrt{\frac{\rho}{6P}}\frac{\Gamma(5/6)\Gamma(1/2)}{\Gamma(4/3)} = 0.91468R_0\sqrt{\frac{\rho}{P}}, \quad (1)$$

where $\Gamma -$ Eulers gamma functions, $\rho -$ density of liquid, P is the pressure at infinity and R_0 the initial value of bubble radius R [].

The basic model is the Rayleigh model [20]:

$$\rho R\ddot{R} + \frac{3}{2}\rho\dot{R}^2 = p_i - p_e, \quad (2)$$

where an overdot means differentiation with respect to time. The difference in pressure, $p_i - p_e$, drives the bubble motion. The form of the inertial terms on the left-hand side is due to the spherical three-dimensional geometry that is transformed to one radial dimension in the differential equation. Both, pi and pe, become functions of radius *R* and time *t*, when gas and vapour fill the bubble, and when surface tension σ, liquid viscosity μ and a sound field, $p(t)$, are taken into account. With these inclusions, the Rayleigh model takes the form [20]

$$\rho R\ddot{R} + \frac{3}{2}\rho\dot{R}^2 = p_{gn}\left(\frac{R_n}{R}\right)^{\kappa} + p_i - p_e - p(t) - \frac{2\sigma}{R} - \frac{4\mu}{R}\dot{R}, \tag{3}$$

with

$$p_{gn} = \frac{2\sigma}{R_n} + p_{stat} - p_v, \tag{4}$$

p_{gn} being the gas pressure inside the bubble at rest, pstat the static pressure and p_v the (here constant) vapour pressure. The pressure $p(t)$is an external pressure applied at the bubble wall. In the case of a single frequency ultrasonic excitation of the bubble, it can be written in the form

$$p(t) = -p_a \sin(2\pi\nu_a t), \tag{5}$$

varying sinusoidally with frequency ν_a and having a pressure amplitude p_a. The '−' sign is convenient for starting the oscillation at $t = 0$ with an expansion of the bubble at rest. This model and some variants are called Rayleigh–Plesset models [20].

A more advanced model is the Gilmore model [20] that incorporates sound radiation into the liquid from the oscillating bubble, whose surface acts like the membrane of a spherical loudspeaker. For strong oscillations, i.e. strong compression of the contents inside the bubble, the model is further augmented by a van der Waals hard-core law to account for a noncompressible volume of the inert gas inside the bubble [20]. This bubble model reads as:

$$\left(1 - \frac{\dot{R}}{C}\right)R\ddot{R} + \frac{3}{2}\left(1 - \frac{\dot{R}}{3C}\right)\dot{R}^2 = \left(1 - \frac{\dot{R}}{C}\right)H + \frac{R}{C}\left(1 - \frac{\dot{R}}{C}\right)R\frac{dH}{dR}, \tag{6}$$

where

$$H = \int_{p_{r\to\infty}}^{p_{r=R}} \frac{dp(\rho)}{\rho}. \tag{7}$$

$$p(\rho) = A\left(\frac{\rho}{\rho_0}\right)^{n_T} - B. \tag{8}$$

$$p_{r=R} = \left(p_{stat} + \frac{2\sigma}{R_n}\right)\left(\frac{R_n^3 - bR_n^3}{R^3 - bR_n^3}\right)^{\kappa} - \frac{2\sigma}{R} - \frac{4\mu}{R}\dot{R}\,. \tag{9}$$

$$p_{r\to\infty} = p_{stat} + p(t). \tag{10}$$

$$C = \sqrt{c_0^2 + (n_T + 1)H}. \tag{11}$$

The additional parameters and variables in this model are the sound velocity in the liquid at normal conditions, c_0, the sound velocity at the wall of the bubble, *C*, the enthalpy, H, the parameters of the equation of state, where the Tait equation (8) is chosen with its parameters *A*, *B*, n_T and the van der Waals constant, *b*. A vapour pressure may be introduced in (9) as in (3) and (4).

A further model is the Keller–Miksis model [20] that also incorporates sound radiation from the oscillating bubble, but features a retarded time $t - R/c$ in the equations. A model equivalent to this model to first order in $1/c$, c being the sound velocity in the liquid, and dispensing with the retarded time reads

$$\left(1 - \frac{\dot{R}}{c}\right)R\ddot{R} + \frac{3}{2}\left(1 - \frac{\dot{R}}{3c}\right)\dot{R}^2 = \left(1 + \frac{\dot{R}}{c}\right)\frac{p_1}{\rho} + \frac{R}{\rho c}\frac{dp_1}{dt}, \tag{12}$$

with

$$p_1 = \left(p_{stat} + \frac{2\sigma}{R_n}\right)\left(\frac{R_n}{R}\right)^{3\kappa} - \frac{2\sigma}{R} - p_{stat} - p(t) - \frac{4\mu}{R}\dot{R}, \tag{13a}$$

$$p(t) = -p_a \sin(2\pi\nu_a t). \tag{13b}$$

Here, too, a van der Waals law may be introduced as in (9) for the gas inside the bubble or a vapour pressure as in (3) and (4). The connection between the different bubble models has been explored by

Prosperetti and Lezzi [20]. Typical values of the parameters for gas bubbles in water, as used in the calculations with the Keller–Miksis model, are p_{stat} = 100 kPa, p_v = 2.33 kPa, σ = 0.0725 $N\ m^{-1}$, κ = 1.67 (noble gas), μ = 0.001 $Pa\ s$, c = 1500 $m\ s^{-1}$ and ρ = 998 $kg\ m^{-3}$. The radius of the bubble at rest, R_n, covers the range from below a micrometre (nanobubbles, microbubbles) to several millimetre, but may reach large values in underwater explosions, either by underwater sparks or with explosives. The driving frequency, va, typically takes values from a few hertz to a few megahertz, but may extend into the gigahertz range. The driving pressure amplitude, p_a, may vary between zero pascal (no sound field) and several megapascal. Theory will not be stretched beyond the three basic bubble models (Rayleigh–Plesset; Gilmore; Keller–Miksis), as they give an astonishing precise description of most experiments on spherical bubble oscillation [20].

These theories are using for all sources of excitation of shock waves in liquids without exception. It can be both acoustic and light stimuli.

Light induced bubbles come with a shock wave upon generation as the material of the fluid is strongly heated [20] and develops a high pressure that is radiated into the liquid. The bubble expansion follows on a slower time scale. These bubbles have various lifetime. Their lifetime is determined by the formula.

$$T_c = 0.915 R_{max} \sqrt{\frac{\rho}{p_{stat} - p_v}}. \quad (14)$$

Equation (14) is modified Rayleygh equation (1).

These models do not include the background history of bubbles and possible channels of conversion of incident radiation. Despite this, it satisfactorily explains the experimental results on the emergence and evolution of bubbles in liquids.

The first thing that comes to mind is that the focused radiation should form diffraction circles, which leads to diffraction delamination of the incident laser beam (Fig. 1 – Fig. 3). In other words, thin layers of intense interaction of initial radiation with matter are formed.

Since the initial radiation is focused, it causes the occurrence of heterogeneous polarization of the medium, which in turn is the source of generation of a whole range of non-linear optical effects, which leads to a continuous spectrum. However, since the cone of initial radiation is transformed into a set of diffractionally stratified cones of heterogeneous polarization of the medium. Then the radiation occurs inside the cones, the generators of which are perpendicular to the generator cones of polarization. And this, according to A. Bohr [26] hyperboloid, is Cherenkov radiation.

The first laser-induced filaments were received in the liquid. Later researches shown that analogous phenomena are generated in solid and gas matter too. Therefore, first models were created for the nonlinear Kerr media and were used for all types of irradiated matter [7, 8]. Strongly speaking, these filaments are sparks of optical breakdown. More universal concept is physical-chemical.

However, Kerr media are represented liquids basically. For solid state basic phenomena are laser-induced electrostriction [22]. In the gas case we can have other nonlinear optical phenomena. Therefore, we must select more universal concept for the determination P_{cr}. It may be physical-chemical method. In this case, we must have concentration of proper centers of scattering (absorption) of laser radiation, which are generated proper nonlinear optical phenomenon, and its activation energy. The self-focusing is nonlinear optical process therefore, P_{cr} or the critical value of energy may be determined in next way. Volume density of energy of the creation self-focusing process may be determined with help next formula W_{crvol} [7, 8]

$$W_{crvol} = E_a N_{nc}, \quad (15)$$

where E_a – energy of activation proper "nonlinear" centers; N_{nc} – their concentration.

Surface density for optical thin may be determined as [7, 8]

$$W_{crsur} = {W_{crvol}}/{\alpha}, \quad (16)$$

where α – absorbance index. Integral value of energy may be determined as [7, 8]

$$W_{crin} = W_{crsur} \cdot S, \quad (17)$$

where S – the square of irradiation.

In this case [7, 8]

$$P_{cr} = {}^{W_{crin}}/_{\tau_{ir}}, \quad (18)$$

where τ_{ir} is duration of laser irradiation.

The determination the concentration of scattering centers must be determined with conditions of proper experiment. It is determined by the conditions of observation the proper phenomena.

Next step of determination the density of energy in our cascade is condition of diffraction stratification. This condition may be determined with help of sizes the diffraction rings. We can estimate density of energy in plane of creation the diffraction stratification for *n*=5.

The explanation of creation the laser-induced filaments have various interpretation. Firstly [7, 8] is the creation wave-guide zones after point of collapse. In this case filaments have little life-time.

Conic part of filament radiation has continuum spectrum: from ultraviolet to infrared. At first this effect was called superbroadening. Therefore, it may be interpreted as laser-induced Cherenkov radiation [7, 8]. The angle 2θ in the vertex of an angle of Fig. 5 (e) is double Cherenkov angle. In this case we have frozen picture of laser-induced destruction of 4H-SiC with help Cherenkov radiation [7, 8].

The Cherenkov radiation is characterized by two peculiarities [7, 8]: 1) creation of heterogeneous shock polarization of matter and, 2) radiation of this polarization. The methods of receiving shock polarization may be various: irradiation by electrons, γ-radiation, ions and excitation with help pulse fields. The stratification of this radiation on other type's radiation (volume, pseudo-Cherenkov a.o.) has relative character and may be represented as laser-induced Cherenkov radiation. Therefore in future we'll be represent conical part of filament radiation as Cherenkov.

This fact may be certified with macroscopic and microscopic ways [7, 8].

First, macroscopic way may be represented according to [27]. The similarity between charge particle and light-induced Cherenkov radiation one can invoke the analogy between Snell's law and Cherenkov radiation [27]. This natural since both effects can be derived in the same way from the Huygens interference principle. In [27] the point of intersection of a light pulse impinging at an angle φ on a boundary between two media moves with velocity $V = {}^{c}/_{n_1 \cos\varphi}$. This relation with Snell's law, gives the Cherenkov relation (Golub formula)[27].

$$\cos\theta = {}^{c}/_{n_2(\omega)V}. \quad (19)$$

This formula allows explain the angle differences for various type of Cherenkov radiation. In this case *V* may be represented as velocity of generation the optical-induced polarization too [7, 8].

The microscopic mechanism of laser-induced Cherenkov radiation is expansion and application of Aage Bohrs microscopic theory of Cherenkov radiation as part of deceleration radiation on optical case [7, 8, 26]. For optical case the Bohrs hyperboloid must be changed on Gaussian distribution of light for mode TEM_{00} or distribution for focused light of laser beam [7, 8]. In this case Cherenkov angle may be determined from next formula

$$\theta_{ch} + \alpha_{ir} = {}^{\pi}/_{2} \text{ or } \theta_{ch} = {}^{\pi}/_{2} - \alpha_{ir}, \quad (20)$$

where α_{ir}– angle between tangent line and direction of laser beam.

Angle α_{ir} was determined from next formula [7, 8]

$$tan\alpha_{ir} = {}^{d_b}/_{l_f}, \quad (21)$$

where d_b – diameter of laser beam, (7 *mm*), l_f – length of focusing or self-focusing. In our case α_{ir} is angle of focusing or self-focusing.

This formula is approximate for average angle α_{ir}.

The Golub formula (19) was used for the determination product $n_2(\omega)V_{nlpol}$ [7, 8]. Self–focusing and Cherenkov angles and product $n_2(\omega)V$ were estimated for *LiF*, CaF_2, fused silica, water and glass BK-7 in [7].

Thereby microscopic modified A. Bohr theory and macroscopic Golub model are mutually complementary methods [7, 8].

The decreasing of Cherenkov angle and product $n_2(\omega)V$ for increasing of laser radiation intensity are corresponded to increasing of nonlinear refractive index and decreasing of velocity of polarization (multiphotonic and multiwave processes) [7, 8].

In completely microscopic mechanism of laser-induced Cherenkov radiation may be represented as nonequilibrium spectrum of all possible Nonlinear Optical phenomena in the local points of propagation the laser beam [7, 8, 20]. It may be Raman and Brillouin scattering, up- and down-conversion, generation of harmonics and various interference of these processes and phenomena, which are generated the continuous spectrum from ultraviolet to infrared regions [7, 8].

The estimation of sizes the cascade of volume destructions of Fig. 5 c) may be explains in next way [7, 8]. The sizes (diameters) of proper stages d_{nir} of cascade are proportionally to corresponding diffraction diameters d_{ndif}

$$d_{nir} = k\, d_{ndif}, \tag{22}$$

where *k* is the proportionality constant.

The diffraction diameters d_{ndif} may be determined with help condition of diffraction-pattern lobes (modified Rayleygh ratio)

$$d_{ndif} = n\lambda. \tag{23}$$

The estimations of first five diffraction diameters d_{ndif} for λ = 800 *nm* were represented in [7, 8].

The distance between diffraction spots and proper moving foci may be determined with help next formula [7, 8]

$$l_{nf} = \frac{d_{ndif}}{2\tan{}^{\varphi}/_{2}}. \tag{24}$$

These distances for φ_1 = 20º and φ_2 = 30º were represented in [7]. In general case the angle φ is depended from homogeneity of irradiated matter or intensity of irradiation.

Qualitative explanation of development of cascade the destructions may be next. The focus of each diffraction zone (spot) is the founder proper shock optical breakdown. But foci with more high number may placed in the "zone" of influence of previous foci. Therefore, only first stage of Fig. 5 (c) is represented pure shock mechanism (Mach cone). Mach cones are characterized the second and third stages of Fig. 5 (c). But its maximums are displaced from center. It may be result if interaction second and third shock waves with previous shock waves: first – for second wave and first and second for third wave. The chock mechanism of destruction certifies a linear direction of optical breakdown. This direction is parallel to direction of shock wave and radiated spectrum is continuum as for Cherenkov radiation and as for observed laser-induced filaments in water and air [4, 8]. Thus, basic creator of optical breakdown traces is secondary Cherenkov radiation and shock waves. This radiation is absorbed more effectively as laser radiation and therefore the creation of optical breakdown traces is more effectively as for beginning laser radiation. Cherenkov radiation is laid in self-absorption range of 4H-*SiC*, but 800 *nm* radiation – in intrinsic range. For the testing of this hypothesis we must measure the spectrum of secondary radiation. In this case we can use physical-chemical cascade model of excitation the proper chemical bonds of irradiated matter in the regime of saturation the excitation [7, 8].

The conclusion about diffractive stratification of focused radiation may be certified by experimental data of Fig. 5 (c).

We can rough estimate basic peculiarities of energy distribution in Mach cone may be used next formula [7, 8]

$$E_{1ob} = \frac{\pi^2}{4}\left(\sum_{i=1}^{5} n_{iav}^2\, l_{iav}\right) r^2 N_{aSiC} E_{Zth}, \tag{25}$$

where n_{iav}– average visible number of filaments in proper group of cascade, l_{iav}=1000 *nm* – average length of filaments in proper group of cascade, r = 10 *nm* – average radius of filament, N_a – atom density of 4H-*SiC*.

The atom density of 4H-*SiC* may be determined with help next formula [30]

$$N_a = \frac{n\rho N_A}{A}, \tag{26}$$

where ρ – density of semiconductor, N_A – Avogadro number, A – a weight of one gram-molecule, n – number of atoms in molecule. For 4H-*SiC* $N_{aSiC} = 9.4 \cdot 10^{21} cm^{-3}$.

For further estimation we use next approximation $n_{1av} = n_{2av} = n_{3av} = n_{4av} = n_{5av} = 100$, (see Fig. 5 (c)).

Energy, which is necessary for the optical breakdown our nanotubes may be determined in next way. Zeitz threshold energy for 4H-*SiC* is equaled $E_{Zth} \sim 25\ eV$ [31]. Let this value is corresponded to energy of optical breakdown. Therefore, summary energy E_{1ob} is equaled

$$E_{1ob} = N_{asnt} \cdot E_{Zth} = 23.2\ nJ. \tag{27}$$

This value is equaled of ~ 8% from pulse energy or ~ 30% from the effective absorbed energy of pulse. In this case we have more high efficiency of transformation initial radiation to "irreversible" part of Cherenkov radiation. It is result of more intensive excitation comparatively with classical methods of receiving the Cherenkov radiation. In this case we have pure photochemical processes. The experimental data for intrinsic absorption (Fig. 4 – Fig.6) show that for short pulse regime of irradiation (femtosecond regime) basic processes of destruction the fused silica and calcium fluoride are photochemical (multiphoton absorption in the regime of saturation the excitation). Nevertheless, basic peculiarity of experimental data Fig. 5 and Fig. 6 is transformation the initial laser radiation (wavelength 800 *nm*) to continuum Cherenkov radiation. From length of optical breakdown in 4H-SiC we can determine average absorption index of Cherenkov radiation. It is ~ 10^4 cm^{-1}. This value is corresponded to violet-blue range of absorption spectrum of 4H-*SiC* [7, 8].

The difference between generations of surface continuum radiation [8] and optical-induced Cherenkov radiation is next. At first time we have collective electromagnetic processes, which are may be represented as processes with velocity less as phase speed of light in media. Mainly, it is wave processes. In the case of Cherenkov radiation, we have directed quantum optical processes, which can have represented as processes with velocity more as phase speed of light in matter. Roughly speaking last processes may be having velocity less as phase speed of light in media but it must be local (quantum) [7, 8]. But in this case we must determine the new phase speed of light as speed of collectivization of electromagnetic oscillations for corresponding frequency in irradiated media because we have continuum spectrum of irradiation. In this case, the summary speed of interaction light and matter is determined the summary time of corresponding chain of direct optical processes.

Cherenkov radiation may be represented as back process of Nonlinear Optics too. Roughly speaking Nonlinear Optics is optics of nonlinear polarization. However, intense laser irradiation is generated nonlinear polarization and Cherenkov radiation [7, 8]. Therefore, these processes have identical nature [8].

We can estimate chain of critical value of energy for the 4H-*SiC* from physical-chemical point of view too.

Critical value of energy, which is necessary for the beginning of self-focusing, may be determined in next way. Volume density of energy of the creation self-focusing process may be determined with help formula (15). In further we made next approximation [7]: $E_a = h\nu = 1.5\ eV$. Then we have for *SiC* $W_{crvol} = 2.4 \cdot (10^{-5} - 10^{-3})\ {}^{J}/_{cm^3}$.`For *SiC* α = 0,1 cm^{-1}. And $W_{crsur} = 2.4 \cdot (10^{-4} - 10^{-2})\ {}^{J}/_{cm^2}$.

Integral value of energy may be determined according by formula (9). For Fig. 5.6(c) for $r = 2\ \mu m$, S = 1,256·10^{-7} cm^2. Therefore $W_{crin} = 3.0 \cdot (10^{-11} - 10^{-9})\ J$. For $r = 1\ mm$ we have $W_{crin} = 1.9 \cdot (10^{-6} - 10^{-4})\ J$.

These estimations are corresponded to estimations, which are received with help formulas for Kerr media. Roughly speaking they are equaled [7, 8]. For the gases this method allows to estimate the energy of its optical breakdown.

Next step of determination the density of energy in our cascade is condition of diffractive stratification. This condition may be determined with help of sizes the diffractive rings. We can estimate density of energy in plane of creation the diffractive stratification for n = 5.

Maximum diameter of diffractive pattern is determined for fifth diffractive ring. For this case average density of energy in plane of diffractive rings is equaled.

We can estimate corresponding correlation between energies for the next processes: laser irradiation, diffractive stratification, Cherenkov radiation and optical breakdown [7, 8].

A density of laser irradiation is equaled

$$W_{avdr} = {E_p}/{S}. \quad (28)$$

Where E_p – energy of laser pulse. For E_p = 200 *nJ* and E_p = 300 *nJ* and S =1,256·10^{-7} *cm*^{2} we have next value of W_{avdr} 1,6 *J*/*cm*^{2} and 2,4 *J*/*cm*^{2}. If we multiple these value of the absorbance index of *SiC* α = 0,1 *cm*$^{-1}$ then we are receiving the volume density of energy $W_{avdrvol}$ 0,16 *J*/*cm*^{3} and 0,24 *J*/*cm*^{3}. Really value is 0,4 from represented data (reflectance is 0,6) and are 0,064 and 0,096 *J*/*cm*^{3} [7].

Correlation ${W_{avdrvol}}/{W_{crvol}}$ for real values for *SiC* is equaled from 27 to 2700 [7].

Density of energy of optical breakdown W_{ob} for *SiC* is equaled 18800 *J*/*cm*^{3}. Therefore, correlation ${W_{ob}}/{W_{avdrvol}}$ is equaled 78333 and 117500 [7].

Concept of diffractive stratification allows explaining the surface character of Cherenkov radiation. This radiation is generated in the region of corresponding focused diffractive ring [7, 8].

In our case (Fig. 6 (c)) sizes of our nanovoids are equaled 15 – 20 *nm*. Therefore, we must change "sound" mechanism of creation cavitations bubbles on electromagnetic. Roughly speaking, this problem was resolved with help change speed of sound or speed of light.

The sizes of nanovoids (Fig. 6 (c)) may be determined with help modified Rayleygh model [7-10, 15] and its form – the help methods of continuum mechanics [1-5] in next way.

Nanovoids may be represented as results of the laser-induced laser-induce breakdown and creation of cavitations bubbles [7] too. The light pressure may be determined with help of next formula [22]

$$p_0 = \frac{E_{ir}}{\tau_i c S}, \quad (29)$$

where E – energy of irradiation, τ_i – pulse duration, S – area of irradiation zone, c – speed of light. For circle symmetry

$$S = \pi r^2, \quad (30)$$

where r – radius of laser spot.

For the estimations of maximal radius of nanovoids we must use modified Rayleygh formula [7-10, 15]

$$R_{max} = \frac{2R}{0.915r}\sqrt{\frac{E_{ir}}{\pi\tau_{ir}cE}}, \quad (31)$$

where T_c – the time of creation the nanovoid (bubble), R is radius of nanovoid, r – radius of irradiated zone, E – Young module, E_{ir}– energy of one pulse. τ_{ir} – duration of pulse [7-10, 15].

If we substitute r = 250 *nm*, R = 10 *nm*, E = 600 *GPa* [7-10, 15], E_{ir}=300 *nJ*, τ_{ir} = 130 *ps*, c=3·10^8 *m*/*s*, than have R_{max}=11 *nm*.

The speed of shock waves for femtosecond regime of irradiation is less as speed of sound. However, we have two speeds of sound in elastic body: longitudinal v_{ls} and transversal v_{ts} [7-10, 15]. Its values are determined with next formulas

$$v_{ls} = \sqrt{\frac{E(1-\nu)}{\rho_0(1+\nu)(1-2\nu)}}, \text{ and } v_{ts} = \sqrt{\frac{E}{\rho_0(1+\nu)}} \quad (32)$$

where ν – Poisson's ratio [7-10, 15]. The ratio between of these two speeds is equaled

$$\alpha = \frac{v_{ts}}{v_{ls}} = \sqrt{\frac{(1-2\nu)}{2(1-\nu)}}. \quad (33)$$

However, this ratio must be true for shock waves too. Therefore, for silicon carbide for ν = 0,45 [7-10, 15] α = 0,33. Roughly speaking last ratio is determined the step of ellipsoidal forms of our nanovoids (Fig. 6 (c)).

In [7-10, 15] allow estimating maximal longitudinal and transversal $R_{max,i}, i \in (l,t)$. These values are 6 *nm* and 19 *nm* properly.

In this case, we represented 4H-SiC as isotropic plastic body. For real picture, we must represent hexagonal structure. However, for the qualitative explanation of experimental data of Fig. 6 this modified Rayleygh model allow explaining and estimating the sizes and forms of receiving nanovoids [7, 8].

As we see, for laser-induced breakdown we must include self-focusing processes too. The problem of creation initial inoculating concentration of electrons is one of main problems Nonlinear Optics too. Therefore, we must include in the problem of optical breakdown the heterogeneity materials and heterogeneity of interaction light and matter, including diffraction stratification, generation of continuum radiation (including Cherenkov radiation), interference Cherenkov radiation and direct optical breakdown. These addition factors allow explaining basic peculiarities of interaction laser irradiation and matter, including gases [7, 8]. However, for more long time of irradiation we have second-order processes of disorder radiation, including reradiation and reabsorption [7, 8]. In this case we may be having processes of heating and creation of plasma clouds [7, 8, 12-14, 23]. For shorter regime irradiation a probability of cascade step-by-step laser-induced direct multiphotonic excitation is increased and therefore we have third scenario of these processes [7, 8]. Thus, methods of Relaxed Optics allow integrating processes of radiated and non-radiated relaxation (Nonlinear and Relaxed Optics) of first-order optical excitation in one system and allow explaining processes of laserinduced optical breakdown and shock processes with one point of view. For qualitative explanation of corresponding experimental data we must add using methods by physical-chemical models and methods of diffraction stratification and laser-induced Cherenkov radiation [7, 8]. Laser-induced shock processes have specific peculiarities. In general case we have electromagnetic and acoustic shock processes [7, 8]. Formally, these processes have similar nature. Speed of electromagnetic shock processes (speed of polarization the media in the result of corresponding interaction) must be more as phase speed of light in media. In this case phase speed of light in media has next physical nature: it is speeding of collectivization the electromagnetic oscillations for proper frequency. Roughly speaking it is electromagnetic characteristic of media, which is corresponded to its electron and ion subsystems. Example of this type process is Cherenkov radiation. In this case, we have radiated reaction of media on heterogeneity excitation of media in shock regimes of interactions. Speed of acoustic shock processes (speed of motion proper object in media) must more as speed of sound in media [7, 8]. But speed of sound is media is average heat speed of media, which is connected with atomic structure of media. Examples of these processes are: flight of airplane or rocket in with supersonic speed; various explosions. Roughly speaking, explosions may be characterized as chemical process with speed more as sound speed in media. Mach number is characterized in this case the macroscopic “detonation” of corresponding process. Both processes (electromagnetic and acoustic) are characterized by Much cone, which is created by proper vectors of speed processes or object and speed characteristic of media (polarization or sound) [7, 8]. Laser-induced shock processes may be represented as analogous to acoustic explosions. However, this process is realized with electromagnetic speed. In this case we must have “electromagnetic” explosion as Cherenkov radiation [7, 8]. Due to the similarity of electromagnetic and acoustic processes of kinetic processes, we can use both to estimate the parameters of impact processes, to determine the size of nanovoids, using the electromagnetic modified Rayleigh model (formula (31)) and to determine the shape of nanovoids, acoustic formula (33). The formation the laser-induced shock processes may be explained with help concept of coherent structures of Relaxed Optics [6]. In this case generation of proper shock process may be represented as chain of coherent processes of interaction light and matter with electromagnetic speed. In this case summary speed of chain process must be less as phase speed of light in media but speed of each term of this chain must be more as phase speed of light in media. It is basic peculiarity of formation laser-induced shock processes comparatively with other electromagnetic processes. From point of view the kinetic concept of Relaxed Optics [6] we must have multiphotonic process in the regime of saturation the excitation [7, 8]. In whole the nonequilibrium and irreversible shock processes may be having electromagnetic and acoustic nature [7, 8]. Nature of laser-induced breakdown is determined by speed of energy transfer

from laser irradiation to matter. For impurity mechanisms of absorption, the laser radiation may be realized next scenario [7, 8]:

1) Multiphotonic absorption is comparatively low intensity but time of irradiation is long-run. In this case, we have heating of matter in the region of the absorption of laser radiation and thermal mechanism of optical breakdown. Other words absorptive energy may be represented as heat, which is cause the heating of media and its thermal breakdown. These process is characterized the speed of sound in matter and time of creation the heating of irradiated material is equaled ~ $(10^2 - 10^3)\tau_{ir}$ for millisecond and nanosecond regimes of irradiation [7, 8].

2) Multiphoton absorption is higher, but it may be source of other collective physical phenomena-generation of plasma, which may be used for the breakdown of irradiated matter. It is plasma mechanism of optical breakdown. Time of formation the plasma in irradiate matter is lesser and roughly speaking it determine by the speed of light. In whole, the speed of this process is lesser as phase speed of light in irradiated matter. However, this time is depending from intensity of irradiation too.

3) Multiphotonic absorption is higher as in case 2 and may be source of direct optical breakdown. However, this process must have speed more as phase speed of light in media. The dimensions of the cavities that are formed during electromagnetic and acoustic breakdown are proportional to the square root of the corresponding velocity (formula (31). Taking this into account, the sizes of acoustic voids in silicon microbead will be on the order of a centimeter. The cone of Cherenkov radiation in the optical case is determined by a cascade of successive light scattering and the corresponding nonlinear polarization of the medium. Therefore, the angle of the Cherenkov radiation is perpendicular to the propagation front of the nonlinear polarization. If the system tends to thermodynamic equilibrium, this trend disappears. This is confirming by the fact that there is no big difference between nanosecond (Fig. 4) and femtosecond (Fig. 5 and Fig. 6) irradiation modes. The efficiency of radiation conversion into breakdown energy is on the order of 10-15 percent. In general, this is determine by the integral photon efficiency of the corresponding cascade process. A. Bohr's model can be applying to relaxation-optical processes, since in this case the displacement of atoms is directly proportional to the intensity of excitation. However, in the case of laser irradiation, we have one irradiation cone and a certain number of diffraction cones. Each diffraction cone is a source of Cherenkov radiation defined by a Mach cone, the characteristics of which are determine by the laser-generated nonlinear characteristics of the irradiated medium. The spectrum of Cherenkov radiation in the case of A. Bohr is determined by a set of hyperboloids, i.e. electromagnetic traces of tracks of incoming particles, and with uniform irradiation it will be more or less uniform. In the case of optically induced Cherenkov radiation, the short-wavelength region, as can be seen from Fig. 5 and Fig. 6, will be concentrated near the optical axis. There is formally no difference between acoustic and electromagnetic shock wave processes. However, when forming nanovoids, we are not dealing with wave but quantum multiphoton processes, which ultimately determine the formation of nanovoids.

Laser-induced shock processes have specific peculiarities. In general case we have electromagnetic and acoustic shock processes [7, 8]. Formally, these processes have similar nature.

Speed of electromagnetic shock processes (speed of polarization the media in the result of corresponding interaction) must be more as phase speed of light in media. In this case, phase speed of light in media has next physical nature: it is speeding of collectivization the electromagnetic oscillations for proper frequency. Roughly speaking it is electromagnetic characteristic of media, which is corresponded to its electron and ion subsystems. Example of this type process is Cherenkov radiation. In this case, we have radiated reaction of media on heterogeneity excitation of media in shock regimes of interactions.

Speed of acoustic shock processes (speed of motion proper object in media) must more as speed of sound in media [7, 8, 20]. However, speed of sound is media is average heat speed of media, which is connecting with atomic structure of media. Examples of these processes are: flight of airplaine or rocket in with supersonic speed; various explosions. Roughly speaking, explosions may be characterize as chemical process with speed more as sound speed in media. Mach number is characterize in this case the macroscopic “detonation” of corresponding process.

Both processes (electromagnetic and acoustic) are characterized by Much cone, which is created by proper vectors of speed processes or object and speed characteristic of media (polarization or sound) [7, 8].

Laser-induced shock processes may be represented as analogous to acoustic explosions. But this process is realized with electromagnetic speed. In this case we must have "electromagnetic" explosion as Cherenkov radiation [7, 8].

In whole the nonequilibrium and irreversible shock, processes may be having electromagnetic and acoustic nature [7, 8].

Now we used physical-chemical method of estimation for the modeling experimental data for *KCl* (Fig. 4). Density of atoms of KCl was determined with help formula (5.68) and it equal $3.1 \cdot 10^{22} cm^{-*3}$ Zeits energy for KCl has value ~ 30 *eV* [31].

Results of modeling are represented in [7, 8].

We used next approximations. Photography of Fig. 4 gives a blurry image compared to the bright-field TEM image of Fig. 5. Therefore, we can't see the microstructure of optical breakdown. And we use rough average approximations for diameter $d_{average}$ and length l of cascade laser-induced optical breakdown of Fig. 4 [7, 8]. Volume of cascade was determined as cylinder volume.

Fig. 4 is similar to Fig. 5 c). However, regimes of irradiation of Fig. 4 are similar to mode TEM_{01}. Therefore, we have two channels of generation the cascade of laser-induced optical breakdown.

The distances between bubbles of Fig. 4 (b) are more as between regions of destruction of Fig. 4(c). However, conditions of focusing the radiation in these both cases are equivalence. Therefore, the distances between neighboring bubbles l_2 of Fig. 4(b) and neighboring regions of destruction l_1 of Fig. 5 (c) are connecting by next formula [8]

$$l_2 = \frac{d_{ndif2}\tan\left(\varphi_1/_2\right)}{d_{ndif1}\tan\left(\varphi_2/_2\right)} l_1 = \frac{\lambda_2\tan\left(\varphi_1/_2\right)}{\lambda_1\tan\left(\varphi_2/_2\right)} l_1. \quad (34)$$

In whole, the correlation of this distasnces is depended from wavelength of irradiation and focusing angles, including intensity of irradiation. Which is determined the step o f homogeneity of irradiated matter. If we substitute in formula (34) $\lambda_2 = 10.6\mu m$ and $\lambda_1 = 0.8\mu m$ and $\varphi_1 = \varphi_2$ then we'll receive

$$l_2 = 13.25 l_1. \quad (34\ a)$$

Energy characteristics of irradiation weren't represented in [12] but were reference on [32]. Therefore, we select value 2 *J*/*pulse* from [7, 8]. In this case we have effective using energy. Methods of estimations of energy characteristics of Table 4.1 are rougher as for 4H-*SiC*. But we must suppose that focused laser irradiation has diffraction stratification, generation of Cherenkov radiation and interference of this Cherenkov radiation. On Fig. 4 (b) 5-7 steps of cascade optical breakdown we see. Sources of Cherenkov radiation id diffraction stratified cones.

If this scenario is true, we have as for 4H-SiC effective transformation the energy of laser radiation to cascade of laser-induced breakdown for *KCl* too. This value is 11,6 – 17,4 percents [7, 8].

We can estimate sizes and forms of possible nanovoids for potassium chloride too. Let's take the ratio of the radius of the irradiation zone to the radius of the nanowire as 50. The energy of irradiation is 2 *J*. The duration of irradiation is 50 *ns*. Young's modulus 29.67 *GPa*, Poisson's ratio 0.216.

After substitution, these data to formula (31) we have $R_{maxKCl} = 62.5nm$. Ellipticity of *KCl* nanovoids may be determined from (33) $\alpha_{KCl} = 0.6$.

Let us now estimate the maximum bubble radii for the acoustic case. For this, in formula (5.73), you need to change the speed of light to the speed of sound (31 a).

$$R_{max}^{ac} = \frac{2R}{0.915r}\sqrt{\frac{E_{ir}}{\pi\tau_{ir}c_s E}}, \quad (31\ a)$$

where c_s is speed of sound.

As a result, we get $R_{maxSiC}^{ac} = 1.7\mu m$ and $R_{maxKCl}^{ac} = 28\mu m$. The shape of the voids does not change, they just increase in size by 2-3 orders of magnitude.

If we take the ratio of the acoustic formula (31 a) and the optical formula (31), then for the same irradiation modes we have the ratio

$$\frac{R_{max}^{ac}}{R_{max}} = \sqrt{\frac{c}{c_s}}. \quad (34)$$

However, a comparison with the experimental results (Fig. 5) shows those electromagnetic rather than acoustic processes play the main role in the formation of nanovoids. This is explaining by the fact that in this case a chain of close-range coherent processes of transformation of both optical radiation into the excitation of the medium and the corresponding relaxation of the medium is implemented, in other words, there is a chain of interconnected coherent transformations.

Experimental data of Fig. 7 and Fig.8 are corresponding to acoustic case and therefore, we can use the Rayleygh and its modified hydrodynamical models for its explanation.

4. CONCLUSIONS

1. Main concepts of modeling the laser-induced cavity in Nonlinear and Relaxes Optics are observed.

2. Short review of corresponding experimental data is represented.

3. Short analysis of Rayleygh theory of cavitation and its extensions (Rayleigh–Plesset, Gilmore; and Keller–Miksis models) are discussed.

4. Necessary of transition to chain methods of modeling the shock processes of Nonlinear and Relaxed Optical processes as including of prehistory the cavitation is formulating.

5. Cascade model as variant of this prehistory is analysed.

6. The difference between acoustic and electromagnetic shock processes shown on the example the generation laser-induced nanovoids in silicon carbide and potassium chloride.

7. Comparative analysis of other properties of acoustic and electromagnetic chock processes is representing too.

REFERENCES

[1] https://www.britannica.com/science/cavitation

[2] Chandramouli P. N. (2014) Continuum mechanics, Yes Dee Publishing Pvt. Ltd., New Delhy.

[3] Batra R. C. (2005) Elements of Continuum Mechanics, American Institute of Aeronautics and Astronautics, Reston.

[4] Trokhimchuck P. P. (2018) Continuum mechanics. Vezha-Print, Lutsk (in Ukrainian)

[5] Rayleygh (J. W. Strutt) (1917) On the pressure developed in a Liquid during the Collapse of a Spherical Cavity. The London, Edinburgh and Dublin Philosophical Magazine and Journal of Science. Vol. 34, 94-98.

[6] Trokhimchuck P. P. (2016) Relaxed Optics: Realities and Perspectives. Lambert Academic Publishing, Saarbrukken

[7] Trokhimchuck P. P. (2020) Relaxed Optics: Modeling and Discussions. Lambert Academic Publishing, Saarbrukken

[8] Trokhimchuck P. P. (2022) Relaxed Optics: Modeling and Discussions 2. Lambert Academic Publishing, Saarbrukken-Cisinau; Trokhimchuck P. P. (2022) Relaxed Optics: Modeling and Discussions 2. AkiNik, New Dehly

[9] Trokhimchuck P. P. (2020) In: Laser-induced optical breakdown of matter: retrospective and perspective. In: Advances in Engineering Technology. Ed. Jaivir Sindh, Vol. 4, Ch. 7. New Delhi: AkiNik Publications, 101-132

[10] Trokhimchuck P. P. (2020) Some Problems of the Modeling the Optical Breakdown and Shock Processes in Nonlinear and Relaxed Optics, IJARPS, Vol. 7, Is.5, 17-30.

[11] Yablonovich E, Bloembergen N. (1972) Avalanche Ionization and the Limiting Diameter of Filament Induced by Light Pulses in Transparent Media. Phys. Rev. Lett., Vol. 29, Is. 14, 907-910.

[12] Yablonovich E. (1971) Optical Dielectric Srength of AlkaliHalide Crystalls Obtained by Laserinduced Breakdown, Appl. Phys. Lett., Vol. 19, Is. 11, 495-497.

[13] Yablonovich E. (1974) Self-phase modulation and short-pulse generation from laser-breakdown plasmas.

Phys. Rev. A., Vol. 19, Is. 5, 1888-1895.

[14] Yablonovich E. (1974) Self-phase Modulation of Light in a Laser-breakdown Plasma. Phys. Rev. Lett., Vol. 32, Is. 20, 1101-1194.

[15] Trokhimchuck P. P. (2023) Shork Electromagnetic Processes in Nonlinear and Relaxed Optics. In: Recent Review and Research in Physics. Ed. Jayminkumar Rajanikant Ray, S.S. Sharma, Vol. 4, ch.3. New Delhi: AkiNik Publications, 23-52.

[16] Di Trapani P., Valiulis G., Piskarskas A., Jedrkiewicz O., Trull J., Conti C., Trillo S. (2003) Spontaneously generated X-shaped light bullets. Phys. Rev. Lett., Vol. 91, Is.9, 093904-1 – 093904-4.

[17] Faccio D, Porras M, Dubietis A, Bragheri F, Couairon A, Di Trapani P. (2006) Conical emission, pulse splitting and X-wave parametric amplification in nonlinear dynamics of ultrashort light pulses. Phys. Rev. Lett., Vol. 96, Is. 19, 193901-1 – 193901-4.

[18] Okada T., Tomita T., Matsuo S., Hashimoto S., Ishida Y., Kiyama S., Takahashi T. (2009) Formation of periodic strain layers associated with nanovoids inside a silicon carbide single crystal induced by femtosecond laser irradiation. J. Appl. Phys., Vol. 106, 054307. – 5 p.`

[19] Okada T., Tomita T., Matsuo S., Hashimoto S., Kashino R., Ito T. (2012) Formation of nanovoids in femtosecond laser irradiated single crystal silicon carbide. Material Science Forum, Vol. 725, 19 – 22.

[20] Lauteborn W., Kurz T. (2010) Physics of bubble oscillations. Rep. Progr. Phys. Vol. 77, 106501, 88 p.

[21] Potemkin F. V., Mareev E. I. (2013) Shock waves and cavitation bubbles dynamics as a function of the tightly focused femtosecond laser energy in distilled water and acetone. Scientific Notes of Physical Faculty. Mikhail Lomonosov Moscow State University, 133401, 1-9 (In Russian)

[22] Sharma B. S. (1968) Laser-induced dielectric breakdown and mechanical damage in silicate glasses. Ph. D. Thesis. Simon Fraser University, Burnaby

[23] Veyko V. P., Libenson M. N., Chervyakov G. G., Yakovlev E. B. (2008) Interaction laser irradiation and matter. Force optics, Phyzmatlit, Moscow (In Russian)

[24] Isselin J.-C., Alloncle A.-P. B., Autric M. L. (1998) Laser-induced breakdown in water: process for shock waves generation. High-Poweer Laser Ablation, 363-369.

[25] Wu J., Zhao J., Qiao H., HU X., Yang Y. (2020) The New Technologies Developed from Laser Shock Processing. Material (Basel). Vol. 13, Is. 6, 1453-1476.

[26] Bohr A. (1950) The influence of atoms interactions on the penetration of particles through matter. In: Bohr N. The penetration of atomic particles through matter. Moscow: Inostrannaya literatura, 105-143. (In Russian)

[27] Golub I. (1990) Optical characteristics of supercontinuum generation. Optics Letters. Vol. 15, Is.6, 305-307

[28] Nibbering E. T. J., Curley P. F., Grillon G., Prade B. S., Franco M. A., Salin F., Mysyrowicz A. (1996) Conical emission from self-guided femtosecond pulses in air. Opt. Lett., Vol. 21, Is. 1, 62–64.

[29] Prade B., Franco M., Mysyrowich A., Couairon A., Buersing H., Eberle B., M. Krenz M., D. Seiffer D., Vasseur O. (2006) Spatial mode cleaning by femtosecond filamentation in air. Opt. Lett., Vol. 31, Is.17, 2601-2603.

[30] Baranskyy P. I., Klochkov V. P., Potykevich I. V. (1975) Semiconductor electronics. Reference book. Naukova Dumka, Kiev (In Russian)

[31] Trokhimchuck P. P. (2007) Radiation Physics of Status Solid, Vezha, Lutsk (In Ukrainian)

[32] Beaulieu A. J. (1970) Transversally excited atmospheric pressure CO_2 lasers,. Phys. Lett., Vol.16, is.12, 504-505.

Citation: *Petro P. Trokhimchuck (2023) "To Question about Nature of Laser-Induced Cavitation" International Journal of Advanced Research in Physical Science (IJARPS) 10(5), pp.1-16, 2023.*